

RESEARCH ARTICLE

Monolayer heterojunction interactive hydrogels for high freedom 4D shape reconfiguration by two-photon polymerization

Supplementary File

The interactive photoresist used a stepwise polymerization strategy and flexible material ratio to maintain the chemical functional groups during ultrafast laser-to-matter interactions. The probability of two-photon absorption depended on the square of laser power, non-linear polarization index, refraction of composite photoresist, and photon energy absorption efficiency of photoresist. High instantaneous peak power boosted the density of free radicals, and the C=C double bonds were cleaved to form a robust, elastic polymeric network, and generating local strain around scanned nanowires^[23]. We describe the cross-linking chains to expound the photon chemical hypothesis as follows:

- (i) Photoinitiators decomposed a fraction of free radicals, radicals extracted hydrogen atoms from NIPAM, and PEG-DA to generate transitional radicals (*a* and *b*).
- (ii) Transitional radicals cross-linked with each other to construct a NIPAM-co-PEG-DA precursor.
- (iii) Photon-unstable MC simultaneously absorbed two photons in local laser focus (mild power of 1.5 – 20 mW) to structurally decompose a considerable sum of benzene ring radicals (*R*) in photolysis. The NIPAM-co-PEG-DA cross-linked with TAIC to obtain a composite polymeric network until it consumed up all free radicals.



Where asterisks (*) denote the excited state of electrons after absorbing photon energy; subscripts *n*, *m*, and *i* are random integers, depending on the dispersity of monomers.

The trick of the new self-driven mechanism lies in manipulating functional group's density to accumulate intermolecular-based reconfigurable stress.

Dynamic E_m was data-fitted by averaging stiffness of $\Delta S/\Delta D$ in penetrating and pulling-out processes as Equation VI:

$$E_m = 1/2mP_w T_t (S_+ / D_+ + S_- / D_-) \quad (VI)$$

Where *m*, P_w , and T_t denote coefficients of stiffness-to-Young's modulus, effective laser power, and interaction time, respectively. As such, the bending angle followed the below exponential relationship (Equations VII and VIII), where the angle is $\beta(t)$, *t* denotes time, τ is a time constant determined by the material, and *L* denotes the lateral bending length. The observed curvature, κ , reached $1 \mu\text{m}^{-1}$.

$$\beta(t) = \beta_o [1 - \exp(-t/\tau)] \quad (VII)$$

$$k = \beta / L \quad (VIII)$$

The monolayer nanostructured interactive hydrogels unleashed the capability of 3D stationary micro/nanostructures with dynamic reconfiguration and tunable mechanics. Although high exposure dosage facilitates oligomers to cross-link

into a denser network and more compact conformation, it also weakens the electrostatic effect of carboxylic/hydroxyl/acylamino groups. It hinders the swelling/shrinkage behavior, reducing the degree of responsiveness. Therefore, we suggest mild laser power <20 mW and fast scanning speed >0.5 mm/s during fabrication (Table S2).

Table S1. A brief overview of the existing stimuli-interactive materials

Material	Stimulus	Reversibility	Biodegradation
Poly (<i>N</i> -isopropylacrylamide)-poly caprolactone	Temperature	No	Partial
Poly caprolactone	Temperature	No	Yes
Poly caprolactone-co-pentadecadolactone	Temperature	No	Yes
Polyvinyl alcohol/chitosan	Swelling	No	Partial
Chitosan/polyethylene glycol	Swelling	No	Partial
Polydimethylsiloxane poly urethane/2-hydroxyethyl methacrylate	Swelling	No	Partial
Polydimethylsiloxane cardiomyocytes	Electric	Yes	Partial
Poly (<i>N</i> -isopropylacrylamide)-co-poly polypyrrole	Electric	Yes	No
Poly (<i>N</i> -isopropylacrylamide)-co-poly pani	Electric	Yes	No
Poly (4-vinyl pyridine)-polystyrene	pH	Yes	No
Poly (2-hydroxyethyl methacrylate)-poly (methacrylic acid)	pH	Yes	No
Poly (<i>N</i> -isopropylacrylamide-co-acrylic acid)-polyethylene glycol	pH	Yes	No

Table S2. Available optical parameters of the femtosecond laser system

Objective lenses	Additive power threshold (mW)	Maximum speed ($\mu\text{m/s}$)	Resolution (nm)	Minimum subtractive power (mW)
10	1.5	2020	913	66
20	1.2	1850	725	62
40	0.5	1935	415	58
100	0.2	1715	153	55

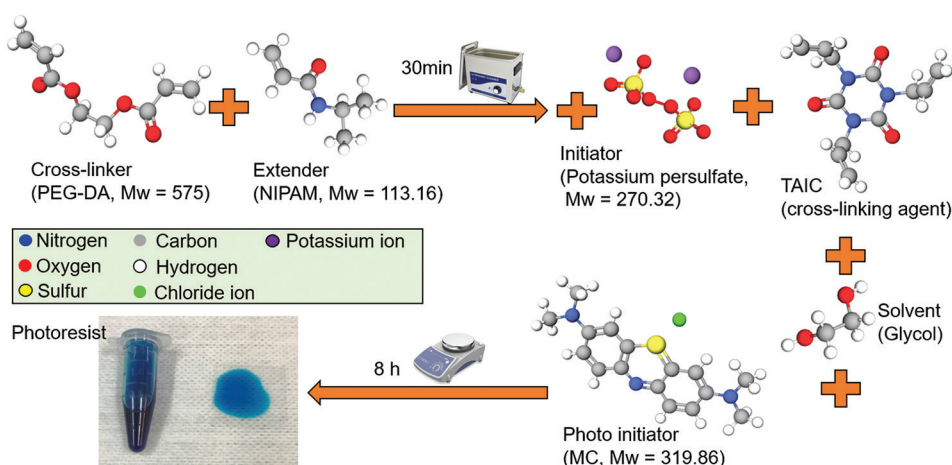


Figure S1. Schematic of preparing photoresist. Centrifugation removed powder sediment. Ultrasonic oscillation/stirring dispersed MC and interactive monomers uniformly in a liquid mixture

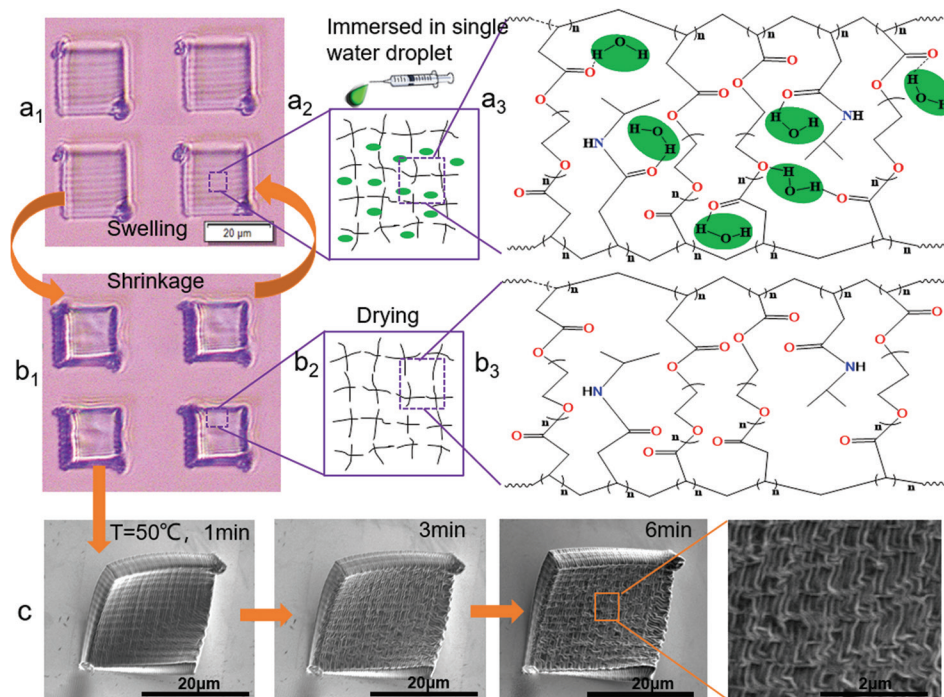


Figure S2. (A₁-A₂, B₁-B₂, and C) The cross-linked hydrogel network interacts with water molecules

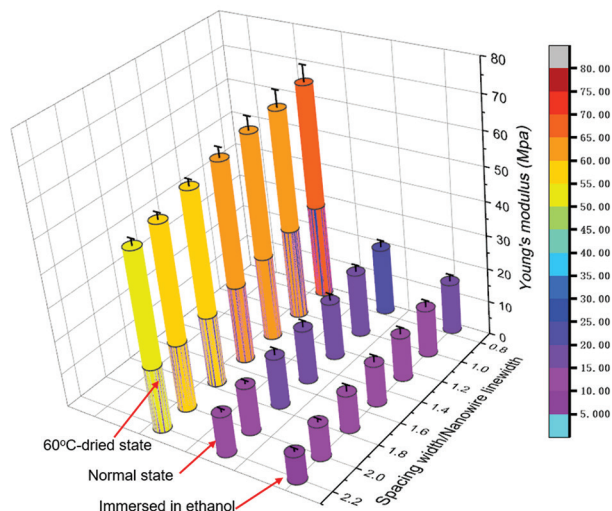


Figure S3. Young's modulus is summarized at three states and different spacing width-to-nanowire line width ratios

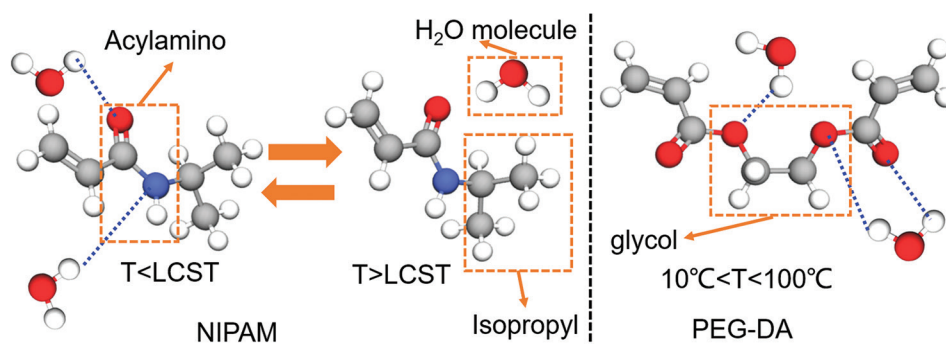


Figure S4. NIPAM contains acylamino functional group to attract water molecules and isopropyl functional group to drive away water molecules. PEG-DA contains a glycol chain for monotonic hydrophilicity

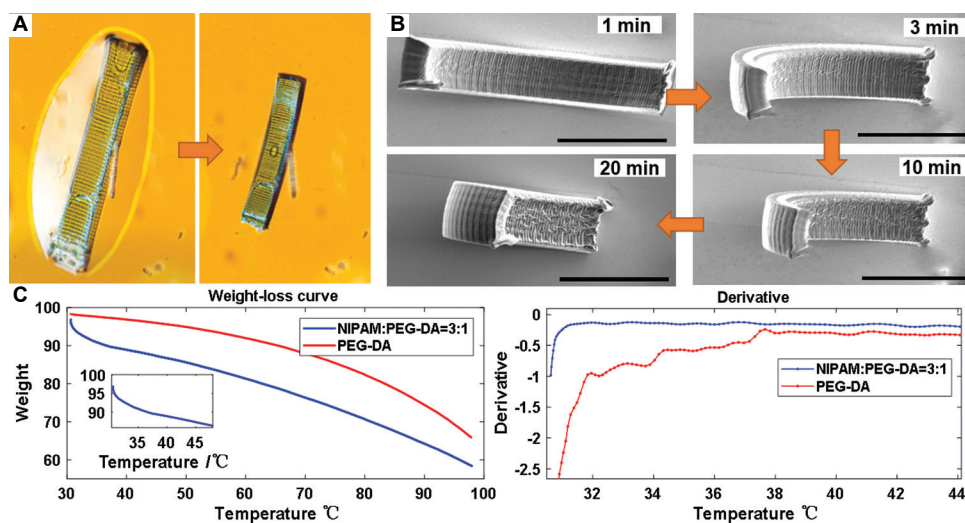


Figure S5. Heat-mechanical curling of a sheet monolayer nanostructured interactive hydrogels and its thermogravimetric analysis. (A) Swelled sheet shrinks to less than half its initial volume. (B) Longer heat time caused a bigger angle upward bending; the scale bar is 30 μm . (C) Weight-loss curve and its derivative in TGA test. Cross-linked hydrogel (blue color) presents substantial weight loss around lower critical solution temperature, $\text{LCST}_{\text{NIPAM}}$. Pure PEG-DA sample showed minor temperature sensitivity within a range of 30 – 45 $^{\circ}\text{C}$

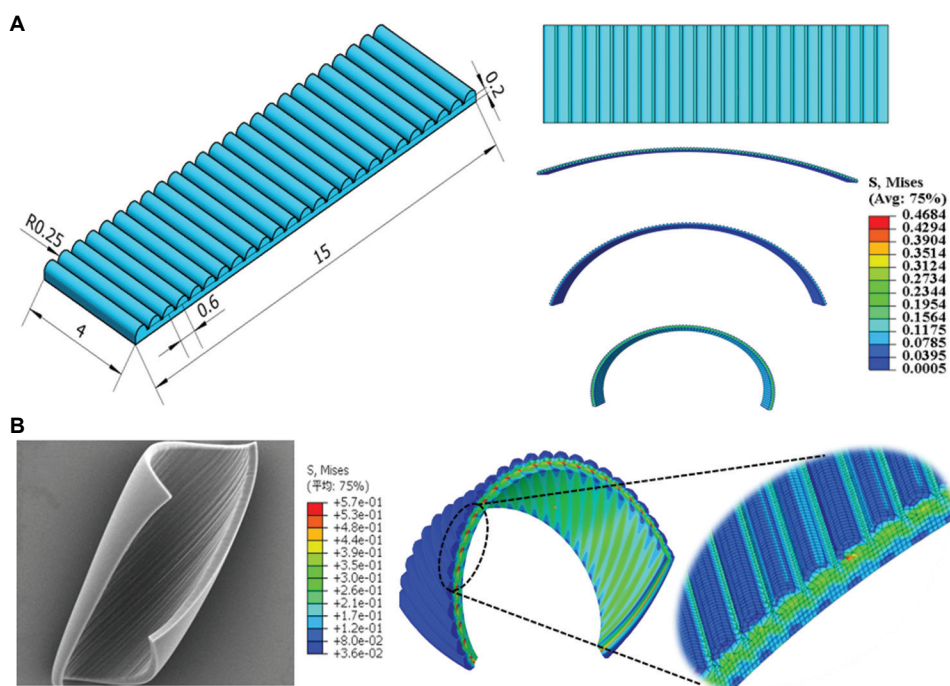


Figure S6. The digital model and numerical simulation of bent monolayer nanostructured interactive hydrogels (MNIHs). (A) Side view and top view of digital models of planar MNIH, and the simulated bending process. (B) Scanning electron microscope image of one bent MNIH sheet and simulation

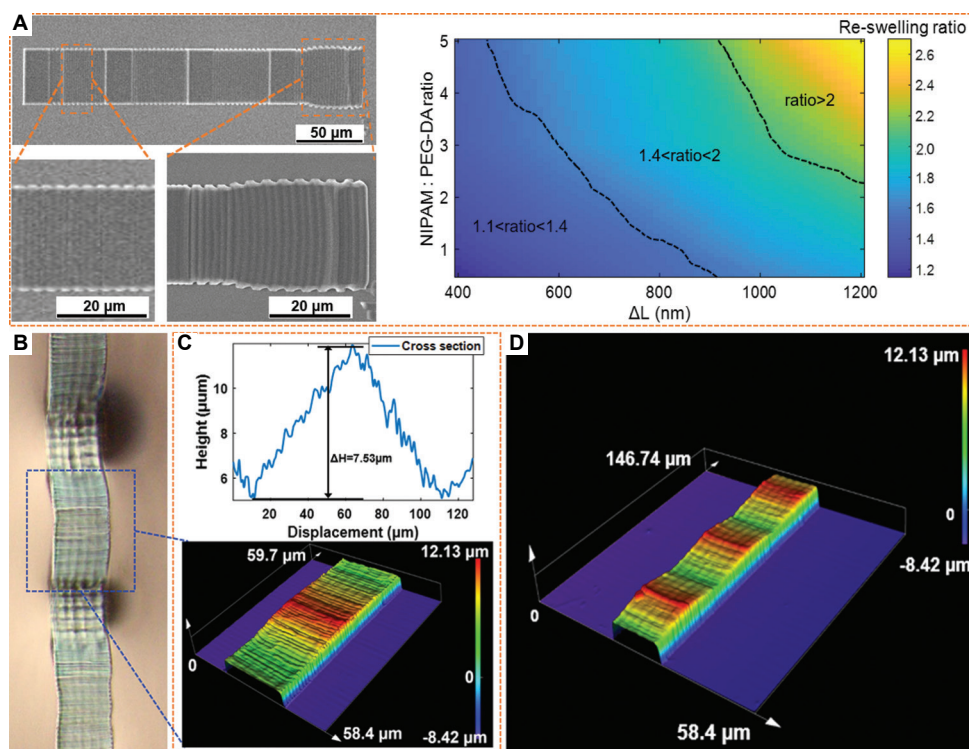


Figure S7. Local swelling and multi-pointed buckling-up programmed by uneven hydrogel nanowires. (A) Wider line pitch results in bigger expansionary dimension, ΔL of re-swelled area, which is approximately 1.6 μm , much bigger than the normal area. (B) Monolayer nanostructured interactive hydrogels (MNIH) buckled up at three local locations; line pitch $\Delta L = 1.6 \mu\text{m}$ was for bigger size-expansion and upward bending, but a bigger adhesion force of $\Delta L = 0.5 \mu\text{m}$ area constrained expansion. (C) Cross-sectional view and SLCM 3D micrograph of a freestanding “bridge” elevated over 7 μm off-substrate. (D) Profile micrograph covering the entire MNIH interface

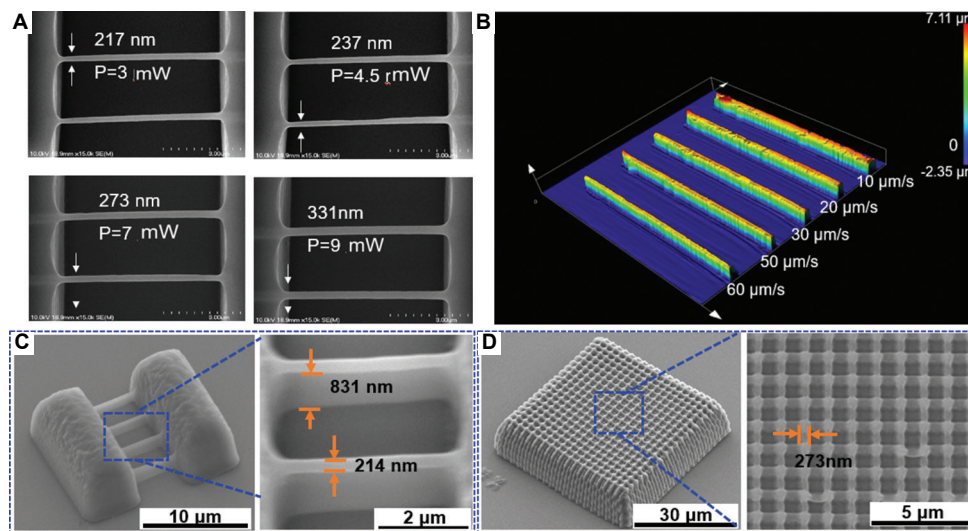


Figure S8. The spatial resolution of single-voxel scanned hydrogel nanowires (NWs). (A) Top view of suspended NWs using different laser powers. (B) Laser confocal microscopy image of NWs laser scanned on the substrate at gradient speeds of 60 ~ 10 μm/s and constant 5 mW power. (C) The width of NWs scanned at different speeds, which increased from 205 to 913 nm at a tunable laser wavelength ($\lambda = 751 \sim 962$ nm). (D) Suspended single-voxel scanned nanowires on air to determine spatial formation resolution

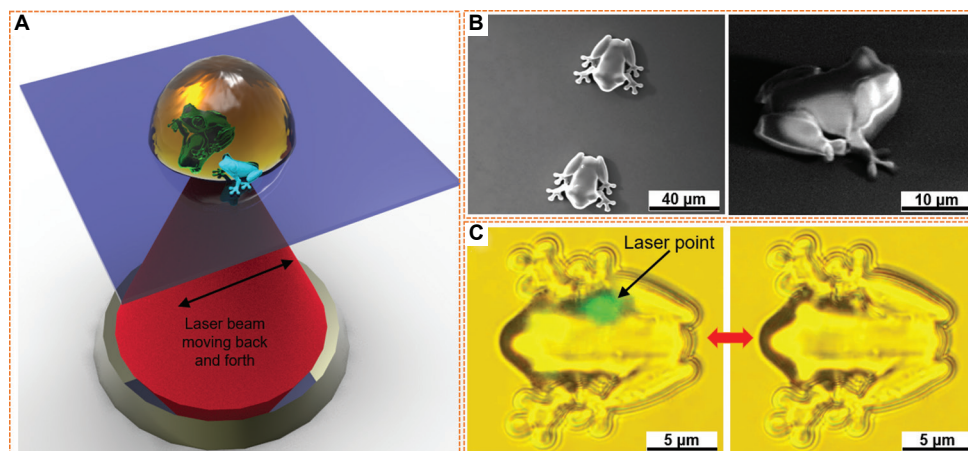


Figure S9. Light-deformable on-chip frog-shaped monolayer nanostructured interactive hydrogels (MNIH). (A) Illustration of light-triggered actuation. The laser beam scanning back and forth on the MNIH. (B) Scanning electron microscope images of frog shape. (C) Laser beam caused local shape-morphing for nodding function also demonstrated in [Videoclip S5](#)

Other files

Videoclip S1. The ultrafast laser system, scanning snowflake, and 2D-to-3D shape reconfiguration

Videoclip S2. Reverse 3D helix self-construction from planar precursor pattern

Videoclip S3. Large-angle opening/closing of C/S-arm tweezer and numerical simulation

Videoclip S4. Non-contact remote light-triggered deformation of frog monolayer nanostructured interactive hydrogels

Videoclip S5. Self-recovery of a “broken heart”/drying-distorted candy/poked woodpile